Online Research @ Cardiff

This is an Open Access document downloaded from ORCA, Cardiff University's institutional repository: https://orca.cardiff.ac.uk/id/eprint/111915/

This is the author's version of a work that was submitted to / accepted for publication.

Citation for final published version:

Maddalena, Riccardo ORCID: https://orcid.org/0000-0001-6251-3782, Roberts, Jennifer J. and Hamilton, Andrea 2018. Can Portland cement be replaced by low-carbon alternative materials? A study on the thermal properties and carbon emissions of innovative cements. Journal of Cleaner Production 186 , pp. 933-942. 10.1016/j.jclepro.2018.02.138 file

Publishers page: http://dx.doi.org/10.1016/j.jclepro.2018.02.138 <http://dx.doi.org/10.1016/j.jclepro.2018.02.138>

Please note:
Changes made as a result of publishing processes such as copy-editing, formatting and page numbers may not be reflected in this version. For the definitive version of this publication, please refer to the published source. You are advised to consult the publisher's version if you wish to cite this paper.

This version is being made available in accordance with publisher policies. See http://orca.cf.ac.uk/policies.html for usage policies. Copyright and moral rights for publications made available in ORCA are retained by the copyright holders.

information services
gwasanaethau gwybodaeth

Journal of Cleaner Production 186 (2018) 933–942

Contents lists available at ScienceDirect

Journal of Cleaner Production

journal homepage: www.elsevier.com/locate/jclepro

Can Portland cement be replaced by low-carbon alternative materials? A study on the thermal properties and carbon emissions of innovative cements

Riccardo Maddalena, Jennifer J. Roberts, Andrea Hamilton*

University of Strathclyde, Department of Civil and Environmental Engineering, Glasgow, G1 1XJ, UK

ARTICLE INFO

Article history:
Received 4 August 2017
Received in revised form
5 December 2017
Accepted 13 February 2018
Available online 19 February 2018

Keywords:
Cement industry
Nano-silica
Carbon footprint
Thermal conductivity

ABSTRACT

One approach to decarbonising the cement and construction industry is to replace Portland cement systems with lower carbon alternatives that have suitable properties. We show that seven cementitious binders comprised of metakaolin, silica fume and nano-silica have improved thermal performance compared with Portland cement and we calculate the full CO_2 emissions associated with manufacture and transport of each binder for the first time. Due to their high porosity, the thermal conductivity of these novel cements is 58–90% lower than Portland cement, and we show that a thin layer (20 mm), up to 80% thinner than standard insulating materials, is enough to bring energy emissions in domestic construction into line with the UK 2013 Building Regulations. Carbon emissions in domestic construction can be reduced by *c.* 20–50% and these cementitious binders are able to be recycled, unlike traditional insulation materials.

© 2018 The Authors. Published by Elsevier Ltd. This is an open access article under the CC BY license (http://creativecommons.org/licenses/by/4.0/).

1. Introduction

Portland cement is one of the most manufactured materials in the world. Over 3 billion tonnes of cement were manufactured in 2012 (Imbabi et al., 2012), and global demand is expected to increase due to the rapid infrastructural development of emerging economies (Schneider et al., 2011; Benhelal et al., 2013). Indeed, global cement production is forecast to reach 3.7–4.4 billion tonnes by 2050, as stated by the World Business Council for Sustainable Development (WBCSD) report in 2009 (Schneider et al., 2011; Benhelal et al., 2013). Cement is primarily used by the construction and geotechnical industries, but there are other emerging applications, including nuclear waste containment, biological and dental ceramics, and water filtration. Cement clinker is produced by calcining limestone (or marl or chalk) with some clay in a furnace at *c.* 1500 °C and is a significant source of greenhouse gas emissions (GHG), which are usually expressed as CO_2 equivalent (CO_{2eq}) and sometimes referred to as "embedded carbon" (Salas et al., 2016). Approximately 900 kg of CO_{2eq} is released per tonne of cement produced by current practices (Hasanbeigi et al., 2010). Thus, the cement industry is estimated to have contributed 5–7% of global anthropogenic CO_2 emissions in 2009 (Turner and Collins, 2013; Hienola et al., 2017). The direct release of CO_2 from calcination during clinker production is responsible for *c.* 50% of the emissions from cement manufacture (Fig. 1). Much of the remaining emissions come from the combustion of fossil fuels for calcination, plus excavation, transportation, milling and grinding processes. Given the global effort to curb CO_2 emissions in an attempt to mitigate dangerous climate change effects (Hienola et al., 2017) (for example the 2015 Paris Agreement, a framework for an internationally coordinated effort to tackle climate change), and the expected rise in global demand for cement, reducing emissions from cement manufacture presents an important challenge. As such, the 'decarbonisation' of cement production is becoming a more prominent issue for the cement sector, as evidenced by the World Business Council for Sustainable Development International Energy Agency (IEA) Cement Roadmap (2009), the Industrial Decarbonisation & Energy Efficiency Roadmaps to 2050 report and the British Cement Association (BCA73 Carbon Strategy 2005) (World Business Council for Sustainable Development, 2009 and 2011, Industrial Decarbonisation and Energy Efficiency Roadmaps, 2015).

Researchers and industry have focused their attention on using alternative fuels in place of conventional fossil fuels (and so reducing the GHG emissions of the traditional manufacturing process), and developing alternative materials by partially

* Corresponding author.
E-mail address: andrea.hamilton@strath.ac.uk (A. Hamilton).

https://doi.org/10.1016/j.jclepro.2018.02.138
0959-6526/© 2018 The Authors. Published by Elsevier Ltd. This is an open access article under the CC BY license (http://creativecommons.org/licenses/by/4.0/).

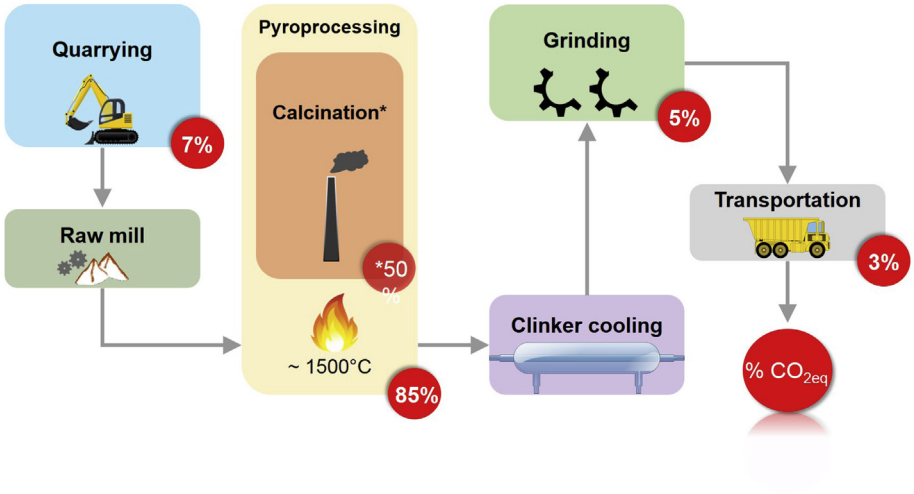

Fig. 1. Simplified diagram of the cement production process. Red circles indicate the percentage of CO_{2eq} emissions associated with manufacturing. (*)50% of the emissions associated with pyroprocessing arise from direct release of CO_2 from calcination and the remaining 35% from fuel and energy consumption. [Image adapted from Imbabi et al. (2012) (Imbabi et al., 2012). (For interpretation of the references to colour in this figure legend, the reader is referred to the online version of this article.)

replacing clinker used in cement systems with waste or by-products (Kajaste and Hurme, 2016). Clinker replacements that have been developed or tested include reused waste, such as industrial by-products like fly ash, or biomass wastes like rice husk ash. Novel binders such as geopolymers or alkali-activated cement (Turner and Collins, 2013; Rostami and Brendley, 2003; Cruz-Yusta et al., 2011; Wu et al., 2015; Sturm et al., 2016; Nie et al., 2016) have also gained popularity. In most cases, clinker is only partially replaced (Hemalatha et al., 2016) but it produces a 'greener' cement. This is advantageous from a regulatory perspective since the existing standardised codes of practice for Portland cement can be adapted or built upon. It is important that the mechanical properties of alternative cements are similar to (or more advantageous than) the properties of Portland cement. Other additives such as silica fume and nano-silica particles improve the properties of Portland cement (Yu et al., 2000; Sanchez and Ince, 2009; Aggarwal et al., 2015; Lazaro et al., 2016) and metakaolin-based geopolymers (Gao et al., 2013; Villaquiran-Caicedo et al., 2015). The main reason geopolymer binders have not yet been more widely adopted by industry is the current lack of regulatory standards backed by long term testing and development (Heidrich et al., 2015).

Portland cement is used in the preparation of mortar for wall rendering/finishing and also in aerated concrete blocks employed as a thermal insulation material (Ahmed and Fried, 2012; Zhang et al., 2014a). However, aerated cement does not offer thermal conductivity values comparable to other solutions on the market, such as polymer foam, glass fibres and vacuum insulation panels (Al-homoud, 2005). Although these materials have very low thermal conductivity, in the range 0.01–0.002 W/(m K) (Cho et al., 2014; Aldawi and Alam, 2016), which can help reduce energy consumption, their production is polluting (Papadopoulos and Giama, 2007; Proietti et al., 2013) plus they cannot entirely be recycled and have to be disposed of in landfill. Geopolymer binders and cement-free mixtures have been proposed as alternative insulation materials to Portland cement-based composites and have shown thermal conductivity values, 0.17–0.35 W/(m K), lower than traditional cement mortar or concrete (0.2–0.8 W/(m K) (Loudon, 1979)) although not comparable with insulation materials such as glass fibres or polymers (Villaquiran-Caicedo et al., 2015).

Life cycle analyses on selected geopolymer binders have found that their use in place of cement could reduce GHG emissions from the cement industry by 9–64% (Turner and Collins, 2013; McLellan et al., 2011). However, these life cycle emissions are context and country dependent and often subject to availability of the raw materials (Stafford et al., 2016a, 2016b; Moretti and Caro, 2017). To date, the environmental sustainability of a range of cement free mixtures has not been comparatively explored, nor has there been a comprehensive analysis of properties of alternative cements and their potential to completely replace Portland cement. Here we consider the carbon reduction that could be achieved by using seven alternative cementitious materials in place of Portland cement, by evaluating the CO_{2eq} gas emissions of Portland cement and geopolymer production and taking the whole life-cycle into account, including the transport of raw materials and the manufacturing process (Imbabi et al., 2012).

The aim of this work is to develop novel 'green' cementitious materials with superior thermal properties to Portland cement and low environmental impact. Silica particles, metakaolin and calcium hydroxide are combined in binary or ternary systems and their physical, thermal and mechanical properties are characterised. Thermal performance is calculated in the context of a typical UK domestic construction and a comparison of GHG emissions for these novel cementitious binders and Portland cement is presented for the first time in the UK-European context. These novel Portland cement free binder represent an environmentally friendly alternative with strong potenital for recycling, a simple manufacturing process and are able to ensure thermal comfort within current international standards. Furthermore, GHG emissions are calculated following a simplified life cycle assessment methodology, which provides a useful decision-making tool to industries or practitioners to rapidly calculate the carbon footprint of Portland cement free binders.

2. Materials and methods

2.1. Materials

Portland cement samples were prepared using Portland cement CEM I 42.5-R (CAS number 65997-15-1), commercially available from the Lafarge Cement Group, and deionised water (W). Physico-chemical properties of Portland cement are listed in Table S1 of the Supplementary Material. Portland cement were prepared with a liquid to solid (l/s) ratio of 0.3:1 using a rotary mixer according to BS EN 196-1:2016 and cast into cubic moulds for 24 h. After 24 h

Table 1
Sample name, mixes and proportions.

Sample	Portland cement	CH	NS	SF	MK	W	NaOH 10 M	NaOH 1 M
	wt%					l/s ratio		
Portland cement	100	–	–	–	–	0.3	–	–
CHI	–	75	–	25	–	0.6	–	–
CHI10	–	75	–	25	–	–	0.8	–
MK10	–	–	–	–	100	–	0.8	–
AMK	–	75	–	–	25	–	1	–
BMK	–	66	–	–	33	–	1	–
MKNS	–	10	5	–	85	–	–	1
CHNS	–	50	50	–	–	2	–	–

samples were kept for 28 days at relative humidity of 98 ± 2% and temperature of 21 ± 2 °C in a nitrogen gas environment to minimise carbonation prior to testing. Novel Portland cement free samples were prepared using different starting materials. Reagent grade calcium hydroxide, $Ca(OH)_2$ (CAS Number 1305-62-0) and Ludox T50 nano-SiO_2 aqueous suspension (CAS number 7631-86-9) were purchased from Sigma Aldrich. Silica fume (CAS number 69012-64-2), commercially available as SF920D from Elkem Microsilica (Norway), was used. Metakaolin was obtained from calcination of kaolin (China clay type purchased from Imerys UK, CAS number 1332-58-7) at 750 °C over 24 h, as described by Alonso et al. (Alonso and Palomo, 2001). Reagent grade sodium hydroxide, NaOH (CAS number 1310-73-2) of nominal concentration 10 M was purchased from Fisher Scientific. Chemical and physical properties of the starting materials (calcium hydroxide (CH), nano-silica (NS), metakaolin (MK), silica fume (SF)) are reported in Table S2 of the Supplementary Material. Given the pozzolanic reactivity of nano-silica and silica fume, binary mixes using calcium hydroxide and silica (nano-silica or silica fume) were investigated (samples CHI, CHI10, CHNS). Alkali activated binders were prepared mixing metakaolin with calcium hydroxide in different proportions. Sodium hydroxide 10M was added as an activator in samples MK10, AMK, BMK and also CHI10, which did not contain metakaolin. Finally metakaolin was mixed with nano-silica and calcium hydroxide, using a lower concentration solution of NaOH (1 M) as the activator (sample MKNS). Mix proportions and sample identification are listed in Table 1. Fresh paste was cast into cubic moulds and specimens were kept for 28 days at relative humidity of 98 ± 2% and temperature of 21 ± 2 °C in a nitrogen gas environment to minimise carbonation. Sample MK10 was thermally prepared following a methodology developed for geopolymers (Zhang et al., 2014b). After mixing, specimens were cast into a cubic mold and kept in an oven at 60 °C and atmospheric pressure for 24 h, then placed in a sealed environment for 28 days at relative humidity of 98 ± 2% and temperature of 21 ± 2 °C.

2.2. Physical, thermal and mechanical properties

After ageing for 28 days samples were removed from the mold and dried at 60 °C to remove pore water and perform mechanical tests and micro-structural analyses. Water removal has an impact on the microstructure, therefore analysis and results presented should be regarded comparatively. Compressive strength testing was performed according to BS EN 196-1:2016, using a uniaxial compressive testing machine at a constant strain rate of 0.4 mm/min until fracture (Sanchez and Ince, 2009; Lin et al., 2010). Three specimens of each composite were tested. The resistance value (Rc) is given in MPa as a mean value of three replicates for each mixing. The heat of hydration was measured using an isothermal calorimeter (I-Cal 4000 HPC, Calmetrix). Fresh paste (c. 60 g) was cast into a cylindrical container and placed into the calibrated calorimeter, at a constant temperature of 21 ± 2 °C. The heat flow was recorded over 80 h. Open porosity (φ) was calculated using the equations reported in the Methods section of the Supplementary Material. Samples were oven dried at 60 °C to constant mass followed by evacuation in a vacuum chamber then saturated overnight with water in the same chamber.

For each sample the laser flash method (LFA) was used to estimate the coefficient of thermal conductivity (λ), given in W/(m·K). A Netzsch instrument 427 LFA was used. Samples of each composition were tested in an argon atmosphere and thermal conductivity was calculated at 25°, 60° and 105 °C according to the BS EN 821-2:1997.

The specimens were powdered and pelletized using an hydraulic press to make pellets of ⌀ 12.7 mm and 3 mm thickness. The surface was coated with graphite to minimise reflectance of the laser beam. A pyroceramic standard supplied by Netzsch was analysed and used as a reference material to calculate the specific heat capacity and thermal diffusivity. Thermal conductivity was calculated at 25°, 60° and 105 °C, as a function of the open porosity, using the equations reported in the Methods section of the Supplementary Material.

In order to evaluate the insulation properties of these novel cement composites, the thermal transmittance (U) of a typical wall was calculated, using the equations reported in the Methods section of the Supplementary Material. An external wall (1 m high and 1 m wide) of standard UK domestic construction was considered, as shown in Fig. 6 (left). The wall consists (from outdoor to indoor) of horizontal bricks (225 × 112 × 65 mm BS EN 771-1:2011, $\lambda = 0.84$ W/(m K)) with a 5 mm layer of cement mortar ($\lambda = 1.4$ W/(m K), Cho et al., 2014) and externally finished with an 18 mm thick layer of mortar render ($\lambda = 1.4$ W/(m K)). Moving inwards from the outer brick skin is a 20 mm thick air cavity ($\lambda = 0.03$ W/(m K)), 9 mm layer of plywood ($\lambda = 0.14$ W/(m K)), a 40 mm thick rock-wool insulation wall ($\lambda = 0.04$ W/m·K, Al-homoud, 2005) and a 15 mm thick gypsum plaster board ($\lambda = 0.21$ W/(mK)) (Cho et al., 2014),)finished with 2 mm thick layer of waterproof plaster paint ($\lambda = 0.09$ W/(m K) (Cho et al., 2014),). This is a pattern in the construction that repeats itself every 70 cm in the vertical direction. Therefore a 1 m wide and 0.7 m high portion of the wall was considered, as it is representative of the entire wall. One-directional heat transfer and constant thermal conductivity values are assumed.

2.3. Powder X-Ray diffraction and Scanning Electron Microscopy

Powder XRD analyses were performed using a Bruker D8 Advance diffractometer with CuKα radiation over the range 5–60° 2θ, step size of 0.02° 2θ and 0.5 s/step. DiffracEva software from Bruker was used for XRD pattern evaluation and phase identification. Microstructural analysis of samples was carried out using Scanning Electron Microscopy (W-SEM, Hitachi S-3700N and FE-

SEM, Hitachi SU6600) with Energy Dispersive Spectroscopy (EDS, Oxford INCA-7260) at an accelerating voltage of 10–15 kV. All samples were resin impregnated, polished and gold coated.

2.4. Greenhouse gas emission assessment

Calculation of the total greenhouse gas emission (GHG), expressed as carbon dioxide equivalent (CO_{2eq}) per 1000 kg of cement produced, takes into account the collective contribution of CH_4, NOx, SOx, CO_2 and synthetic gases emitted during production of the material, including excavation and transport of raw materials and reagents, and manufacturing. The approach to estimate the total GHG is based on the methodology reported in McLellan et al. (2011) and calculated using equation (1):

$$GHG_{Tot} = \sum_{i=1}^{n} m_i(d_i e_i + p_i) \quad (1)$$

where GHG_{Tot} is the total greenhouse gas emission (kg_{CO2eq}) per tonne of material produced, m_i is the fraction of component i, d_i is the distance transported by a given mode of transport (km), e_i is the emission factor for the transportation mode (kg_{CO2eq}/(km tonne)) and p_i is the emissions per unit mass of component i produced (kg_{CO2eq}/tonne). The following assumptions were made in the analysis:

1. The calculations were based on the manufacture of 1 tonne of Portland cement binder and 1 tonne of cement free materials in the United Kingdom, using, where possible, UK products, or otherwise materials from a typical supply chain.
2. Previously published values for CO_{2eq} emissions from the manufacture of the raw materials were used, and added to the emissions from transport to and within the UK.
3. The emissions due to the addition of water to cement paste are very low (0.271 kg_{CO2eq}/tonne (Reffold et al., 2008)) and so are not taken into account.
4. Maximum distances and mode of transport are selected as those which maximise CO_{2eq} emissions, because this work adopts the worst-case scenario for CO_{2eq} emissions.
5. Emission factors associated with road transport (e_r) and sea transport (e_s) are respectively 0.09 kg_{CO2eq}/(km tonne) and 0.02 kg_{CO2eq}/(km tonne) (McLellan et al., 2011; IPCC, 2006).
6. Emissions per unit mass of Portland cement (p_{PC}) are 750 kg_{CO2eq}/tonne and is produced in mainland UK.
7. Emissions per unit mass of metakaolin (p_{MK}), produced in England and silica fume (p_{SF}), produced in Norway, are respectively 236 kg_{CO2eq}/tonne and 7×10^{-6} kg_{CO2eq}/tonne (McLellan et al., 2011; Duxson et al., 2007).
8. The manufacture of calcium hydroxide is based on the hydration of calcium oxide, produced in Northern Ireland, ($p_{CO} = 750$ kg_{CO2eq}/tonne) taking into account a correction factor of 0.97 due to the addition of water ($p_{CH} = 720$ kg_{CO2eq}/tonne) as explained in the IPCC Guidelines for national greenhouse gas emissions (McLellan et al., 2011; Duxson et al., 2007).
9. Sodium hydroxide is produced in Northern Ireland by a chemical process using electrolytic cells. The emissions associated with the production are in the range 1120–1915 kg_{CO2eq}/tonne as reported for a nominal concentration of 16 M (Turner and Collins, 2013; Mellado et al., 2014; Chan et al., 2016). In order to take into account lower sodium hydroxide concentrations, we used a correction factor of 0.43 and 0.63 respectively for NaOH 1 M and NaOH 10 M on the lowest emission value ($p_{NaOH} = 1120$ kg_{CO2eq}/tonne), following the principle of the IPCC guidelines (IPCC, 2006).
10. The nano-silica suspension is manufactured in Germany and the carbon emissions value can be obtained from the manufacture of sodium silicate solution ($p_{NS} = 386$ kg_{CO2eq}/tonne) (Lazaro et al., 2013, 2016; EU, 2007).

A schematic diagram of mode of transport and distances for each raw material is shown in Fig. 2.

3. Results and discussion

3.1. Physical, thermal and mechanical properties

The particle size and the high specific surface area of nanoparticles play an important role in the physical and mechanical properties. The measured bulk density (ϱ), matrix density (ϱ_{mat}), open porosity (φ), compressive strength (R_c) and cumulative heat released values are reported in Table 2. All the mixes show values of bulk density in the range 600–1100 kg/m^3, much lower than standard Portland cement (1900 kg/m^3). Density and porosity values are in good agreement with literature data on lightweight materials such as calcium silicate boards and aerated concretes (Hamilton and Hall, 2005; Ünal et al., 2007; Palmero et al., 2015). Sample CHI10 shows a higher bulk density and lower porosity compared to sample CHI due to the greater l/s ratio and the presence of an alkaline activator. Samples MK10, AMK and BMK show very similar density and porosity values and porosity is highest when nanosilica is used. Mechanical tests performed on all the samples after 28 days of curing show values of compressive strength, in the range of 1.8–7.8 MPa. Although compressive

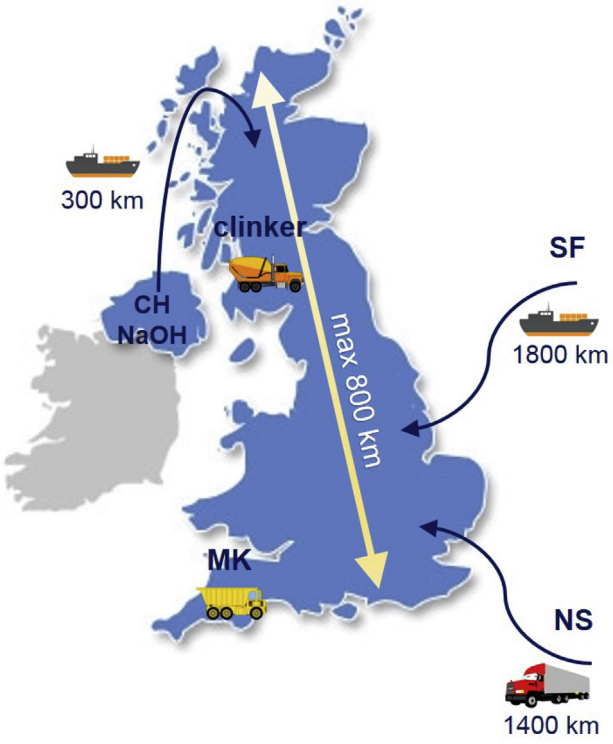

Fig. 2. Diagram of transportation mode and average distance for raw materials in and to UK. Silica fume (SF) is supplied from Norway, nano-silica (NS) from Germany, calcium hydroxide (CH) and sodium hydroxide (NaOH) from Northern Ireland (UK), metakaolin (MK) and Portland clinker are available in mainland UK.

Table 2
Bulk density (ϱ), matrix density (ϱ_{mat}), open porosity (φ), compressive strength (R_c) and cumulative heat release of all the samples.

Sample	ρ kg/m^3	ρ_{mat} kg/m^3	φ –	R_c MPa	Heat release J/g
OPC	1940	2460	0.21	51.2	235
CHI	940	2430	0.61	6.4	44
CHI10	1120	2160	0.48	7.7	211
MK10	1020	2190	0.53	5.2	446
AMK	900	2180	0.59	4.7	75
BMK	850	2020	0.58	6.5	104
MKNS	640	2260	0.72	1.7	51
CHNS	610	2390	0.74	2.2	148

strength values are not comparable with Portland cement, they satisfy the resistance requirement for non-loaded structures and results are similar to the values given for aerated concrete blocks (Al-Jabri et al., 2005; Prakash et al., 2013) and lime-metakaolin mortars (Grilo et al., 2014; Gameiro et al., 2014). Isothermal calorimetry was used to measure the heat flow development of the samples at 21 °C. Fig. 3 shows the heat flow (in mW/g) of the samples compared to Portland cement. Since the mixing was done externally, the first peak appears at the very beginning of the measurement for all the samples (Fig. 3a); it corresponds to particle wetting and dissolution, the chemical reaction which leads to the formation of hydrated phases. The second peak appears broad and delayed compared to Portland cement. It corresponds to the polymerisation of dissolved species into new crystal structures. In sample CHI the first peak converges into a straight horizontal line and no second peak is detected, indicating very low reactivity (Nath et al., 2016). Sample CHI10 shows the influence of the alkali-activator, resulting in higher intensity and accelerated hydration. Specimen CHNS (CH and NS) shows the same trend of mix CHI (CH and SF), with a high first peak converging into a horizontal line. However a second peak is detected as a broad hump at around 20 h. This is due to the smaller particle size and higher reactivity of NS compared with SF. Sample MK10 shows a high-intensity broad first peak followed by small broad hump associated with the second peak of hydration. Samples AMK and BMK have respectively 75% and 66% calcium hydroxide content. In sample BMK, the higher content of MK produces a delay in the second peak compared to sample AMK. The peak is higher in intensity from the increased formation of alkaline aluminosilicate due to the greater concentration of dissolved aluminum ions (Alonso and Palomo, 2001). The

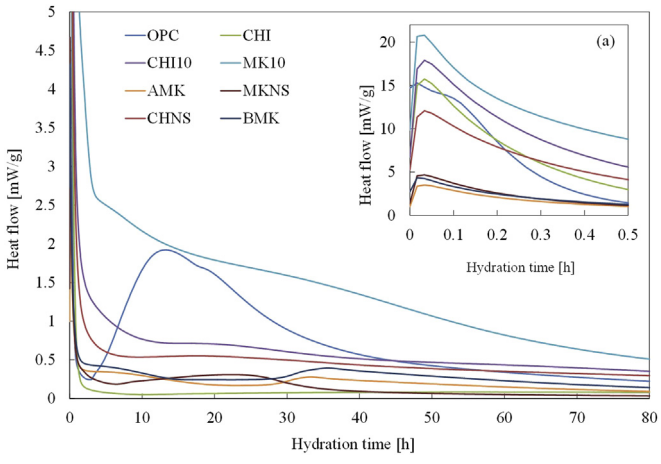

Fig. 3. Heat flow measurement for each sample. (a) Magnification of the first 30 min of heat flow measurement.

cumulative heat released in the first 80 h was obtained by integrating the heat flow curves and is summarised in Table 2. Except for the mix MK10, with a total heat release of 446 J/g, in accordance with the work of Zhang et al. (2012), all the other mixes show a cumulative energy lower than Portland cement. Cumulative heat released is detailed in Table 2 and shown in Figure S1 in the Supplementary Material.

3.2. Powder X-Ray diffraction and Scanning Electron Microscopy

XRD patterns obtained for the developed materials are presented in Figure S2 in the Supplementary Material, where only the major mineral phases are shown. Samples CHI and CHI10 are mainly crystalline portlandite (P) and poorly crystalline calcium silicate hydrate gel (C-S-H), the most abundant component of hydrated cement paste and responsible for early strength development and hardening (Taylor, 1998) or calcium (sodium) silicate hydrate (C-(N)-S-H) (Gomez-zamorano et al., 2016; Gomez-Zamorano et al., 2017). Semi-quantitative analysis of the XRD patterns showed that, despite the high pH, sample CHI10 has 54% C-S-H compared to sample CHI (61%). The added Na^+ concentration requires Ca^{++} to produce C-N-S-H in addition to the C-S-H produced. Some minor carbonated phases are detected, (calcite and sodium carbonate), arising from surface carbonation. In the mixes containing metakaolin and calcium hydroxide (sample AMK, BMK and MKNS), stratlingite (St), calcium aluminate hydrate (C-A-H) and monocarboaluminate (M) phases are detected, in agreement with Silva et al. 2014. Stratlingite is the main hydrate phase responsible for strength development in lime-metakaolin based materials. An increase of metakaolin content from 25% to 33% respectively in samples AMK and BMK results in well defined peaks of stratlingite, and consequently higher compressive strength. Faujasite (F) is the main crystalline compound in sample MK10 along with C-S-H gel, calcium aluminate hydrate and minor stratlingite. In sample MK10, mixing metakaolin with 10 M NaOH solution promotes alkaline activation and leads to the formation of sodium aluminum silicate hydrate (N-A-S-H) gel and the secondary formation of faujasite (F) (Zhang et al., 2014b; Reig et al., 2016). In sample MKNS, reducing the concentration of the activator from 10 M to 1 M and the addition of calcium hydroxide at ambient temperature results in the precipitation of poorly-crystalline calcium aluminate hydrate (C-A-H), the main phase detected. Sample CHNS presents broad humps at c. 29° and 32° 2θ, typical of C-S-H gel (Garbev et al., 2008).

As shown in the SEM images, the developed materials present a highly porous matrix in agreement with the density and porosity values measured. In sample CHI the matrix is mainly poorly-crystalline C-S-H whereas the presence of NaOH as alkaline activator in sample CHI10 promotes the formation of C-S-H combined with C-(N)-S-H phases, respectively in Fig. 4a and Fig. 4b As shown in XRD patterns, alkali-activation of metakaolin-lime mixes results in formation of calcium aluminate silicate hydrate (stratlingite) and C-S-H (sample BMK, Fig. 4c). Fig. 4d shows a semi-crystalline C-S-H phase forming a complex plate-like structure in sample CHNS.

3.3. Thermal conductivity measurements

Thermal conductivity values at 25°, 60° and 105 °C calculated according to equation S(5) are shown in Fig. 5 and compared to Portland cement. Values are in the range 0.05–0.26 W/(m K), 50–90% lower than Portland cement. Samples made mixing metakaolin and sodium hydroxide (MK10, AMK and BMK) show thermal conductivity values in accordance with Palmero et al. (2015) and Villaquiran-Caicedo et al. (2015). The addition of silica nano-

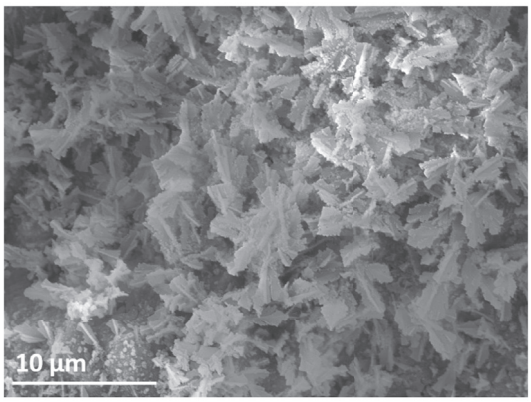

(a) FE-SEM image of sample CHI showing poorly crystalline C-S-H.[Voltage 15 kV]

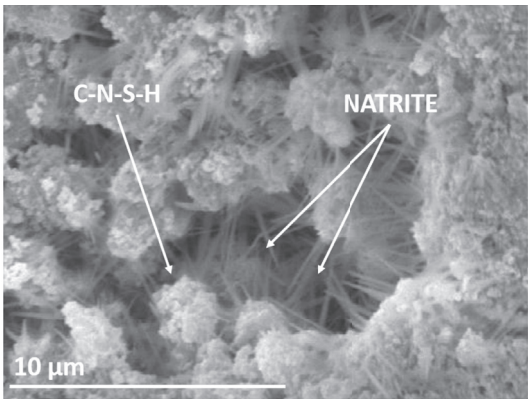

(b) W-SEM image of sample CHI10 showing C-N-S-H and needles natrite. Identification was aided by SEM- EDS analysis. [Voltage 15 kV]

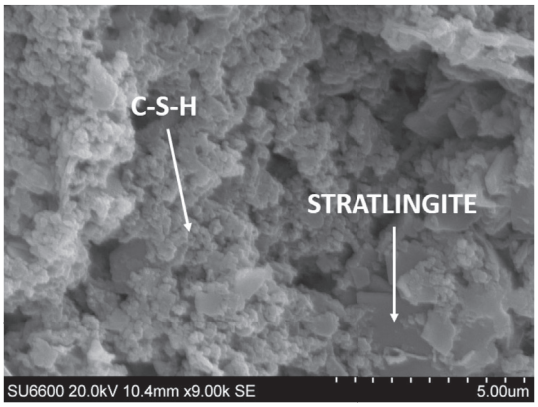

(c) FE-SEM image of sample BMK showing a porous microstructure formed by stratlingite and C-S-H.

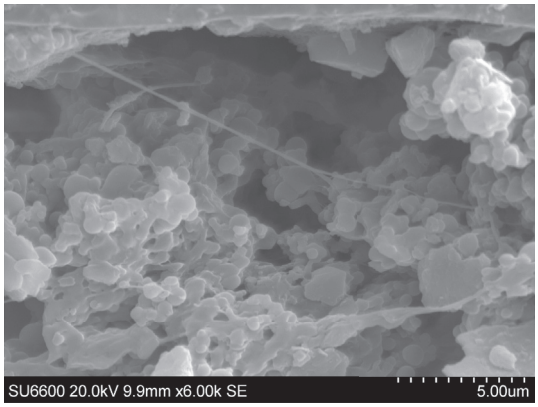

(d) FE-SEM image of sample CHNS showing a porous microstructure formed by plate-like C-S-H phase.

Fig. 4. SEM images of (a) sample CHI, (b) sample CHI10, (c) sample BMK, and (d) sample CHNS.

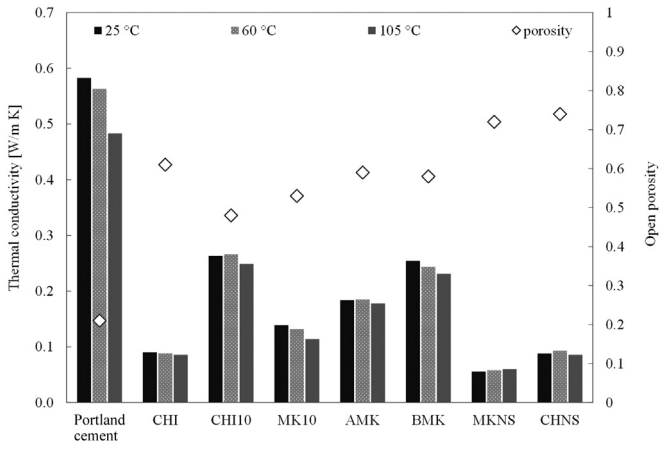

Fig. 5. Thermal conductivity of samples at 25°, 60° and 105 °C and porosity values.

particles has a beneficial effect on the thermal conductivity. Sample MKNS and CHNS in fact show the lowest λ values at 25 °C, 0.055 and 0.088 W/(m K) respectively. These values are typical of insulating materials (Cho et al., 2014; Fricke et al., 2008). This effect is attributed to the smaller nano-silica particle size range and greater surface area, which increases the porosity ($\varphi = 0.7$) but decreases the pore-size; the overall consequence is an enhanced phonon scattering effect which reduces heat transfer (Alvarez et al., 2010). Samples made by mixing CH and SF, either with water or alkali-activated show a different thermal behaviour: while sample CHI has a thermal conductivity value ($\lambda = 0.09$ W/(m K)) similar to CHNS, sample CHI10 has a higher λ, suggesting that the alkali-activator (NaOH, 10 M) contributes to the reduction of porosity but decreases the thermal resistance. As shown in XRD patterns, sample CHI contains C-S-H and portlandite, whereas CHI10 is made of C-S-H, natrite and portlandite, bound together in a denser and less porous matrix (c. 20% less than CHI).

Thermal transmittance (U-value) for a typical wall (Fig. 6) was

calculated to be 0.32 W/(m K), using equations reported in the Methods section of the Supplementary Material. Building Regulation 2013 in England and Wales for refurbishment of existing buildings (domestic and non-domestic use) requires values less than 0.30 W/(m K). The application of a layer of novel cementitious material can contribute to the reduction of the total transmittance below the limit imposed by building regulations, using materials of relatively simple manufacture. The U-value was then calculated taking into account an additional layer of developed material placed in between the bricks and the air cavity. The thickness was chosen in order to minimise the total transmittance below the limit of the building regulations. Thickness values of all the mixes are summarised in Table 3. The thickness of insulation material layers used in the construction industry is in the range of 30–100 mm (e.g. glass fiber, rock-wool or polymeric foam (Cho et al., 2014)). Here, a 20 mm layer of mix MKNS is required to reduce the total transmittance by 10%, as shown in Fig. 6. Conventional insulation materials such as rock-wool, polystyrene or glass fibres, are usually placed in layers of approximately 40–80 mm (Aldawi and Alam, 2016; Bull et al., 2014).

3.4. Life cycle emissions

Previous studies have addressed the need to meet thermal requirements, using thermally resistant polymers or composites, but the carbon footprint associated with their manufacture is often overlooked (Fricke et al., 2008; Alam et al., 2014)). The estimated CO_{2eq} emissions (GHG_i) for each of the seven cementitious material are reported in Fig. 7 and compared to Portland cement. These present the 'worst case scenario', and so the actual CO_{2eq} emissions would likely be lower than those reported here. The carbon footprint of each component material is shown in Fig. 7a. The calculated values are similar to previously published estimates for geopolymer binders and concrete in different contexts Turner and Collins, 2013; McLellan et al., 2011; Mellado et al., 2014, Chan et al., 2016. The results show that all types of novel cements studied here have lower embedded carbon than Portland cement. For example, sample MKNS has the lowest CO_{2eq} emissions associated with its manufacture, estimated to be half the emissions of Portland cement. Sample AMK, which has the highest embedded carbon

Table 3
Minimum thickness of novel cement to achieve *U*-value ≤ 0.29 W/(m^2 K).

Sample	minimum thickness mm
CHI	30
CHI10	80
MK10	50
AMK	60
BMK	80
MKNS	20
CHNS	30

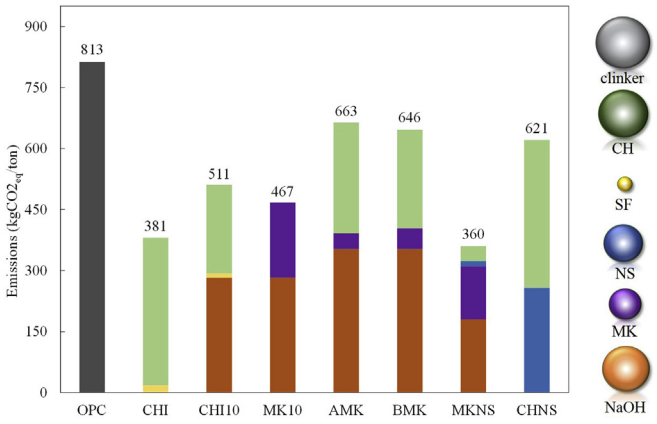

Fig. 7. Total GHG emission and contribution of each raw material for all the mixes. (a) Bubbles indicate the single component in each mix and the size indicates the GHG emission associated: clinker (750 kg_{CO2eq}/tonne), CH (720 kg_{CO2eq}/tonne), SF (0.01 kg_{CO2eq}/tonne), NS (390 kg_{CO2eq}/tonne), MK (236 kg_{CO2eq}/tonne), NaOH 10 M (700 kg_{CO2eq}/tonne), NaOH 1 M (481 kg_{CO2eq}/tonne).

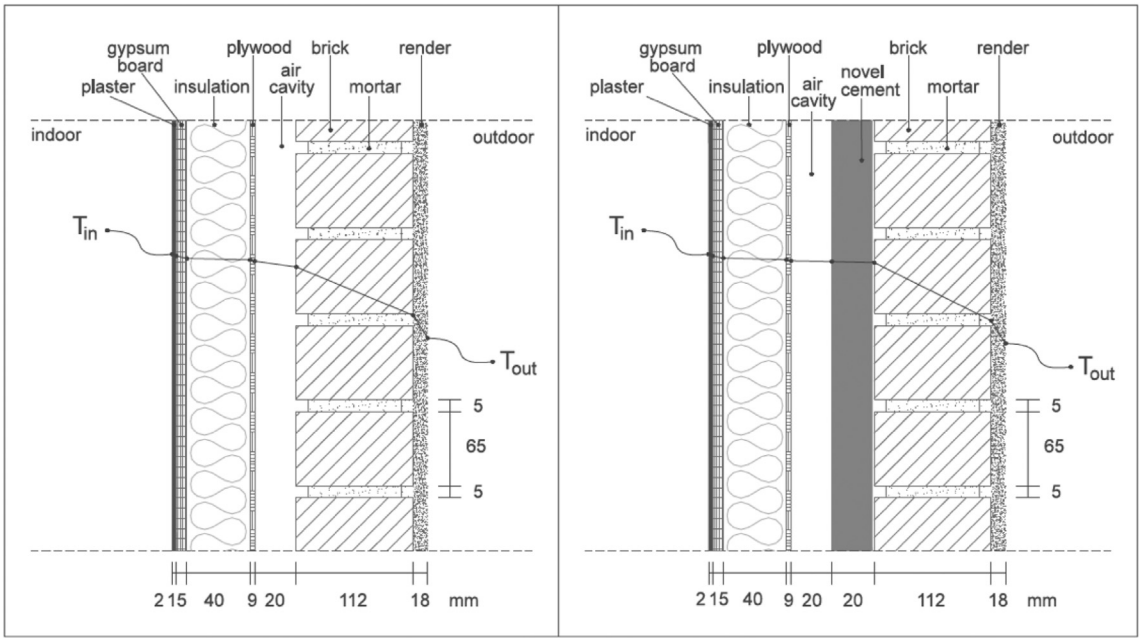

Fig. 6. Typical external composite brick wall of domestic building in United Kingdom. (Left: Wall section and temperature (*T*)profile. Right: Wall-section including a layer of MKNS and temperature profile).

among the novel cements, still has 20% lower CO_{2eq} than Portland cement. The selected raw materials, their world-wide availability coupled with minimum manufacturing make these novel binders environmentally competitive compared to traditional insulators (e.g. 1 tonne of extruded polystyrene is responsible for 1180 kg_{CO2eq}) Papadopoulos and Giama, 2007. NaOH and CH are the most common ingredients of the alternative cements tested here, and the embedded carbon in these materials is similar to clinker (Fig. 7a). Thus, it is the relative proportion of low carbon materials such as SF, MK and NS which determine the overall carbon footprint for each cement. The major energy expended in the manufacture of NaOH occurs in the electrolysis process followed by cooling, which has a large electricity requirement. However, recent findings have proven that natural highly alkaline materials, such as red mud, could be used, with comparatively high mechanical performance Nie et al., 2016. CH is produced by calcination of calcium carbonate followed by hydration. The CO_2 footprint of both materials could be reduced if they were produced using an alternative source of energy for the electricity required (e.g. wind turbine, nuclear energy, photovoltaic energy for the manufacture of NaOH) or using biomass or other green fuel in the pyroprocessing of calcium carbonate.

3.5. Environmental impact

Due to their low thermal conductivity, the novel cements present an environmentally sustainable alternative for purposes such as wall cladding. Improving insulation in homes and buildings is an important aspect of reducing thermal energy loss and thus in turn reducing energy consumption. The innovative binders studied here are also highly recyclable compared to conventional insulating components such as polymeric foams, polystyrene, polyurethane, rock-wool or vacuum insulation panels. They could be re-used in the building industry as intended by the European Waste Framework Directive 2008/98/EC and the EU Framework Programme for Research and Innovation Horizon 2020 which stipulates that up to c. 80% of recycled construction and demolition waste material should be re-used to decrease the content of Portland cement used and consequently reduce the amount of waste to be placed in landfill. Further, they require less manufacturing and processing, and the raw materials and reagents are readily available, which is important to consider for large-scale production.

Thus, although novel cements cannot replace Portland cement in all applications, they offer an environmentally sustainable alternative to traditional materials for several applications, and there is significant potential for these materials to contribute towards the decarbonisation of the cement industry.

4. Conclusions

In this study low-carbon cementitious materials have been developed and characterised. Metakaolin, silica fume, nano-silica and calcium hydroxide were combined at different ratios to produce 'green' binders for construction industry. Physical and mechanical properties were investigated. Compressive strength values (in the range 2–7 MPa) are typical of non-structural cements (mortars, rendering cements, etc.); density and porosity measurements show that these materials could be used in construction industry as functional building elements. Pozzolanic activity was detected by isothermal calorimetry and hydrated phases (calcium/aluminum silicate hydrate, faujasite, stratlingite) were found in XRD diffractograms. SEM images give an insight to the microstructure, with the presence of poorly crystalline phases (i.e. C-S-H) and highly porous matrices, in agreement with the porosity measurements (0.48–0.74). Samples present thermal conductivity (0.05–0.26 W/m K), in the range of conventional insulating materials. While previous studies have focused their attention on solely physical properties of Portland cement-free cements and geopolymers, here we have brought together innovative materials able to satisfy thermal performance requirements within environmental standards. In fact, the addition of a 20 mm layer of sample MKNS to an external wall of existing housing, contributes a 10% decrease in thermal transmittance, as required by the Building Regulation 2013 in England and Wales. The environmental impact of these new cements was assessed, including estimating the greenhouse gas emissions associated with their manufacturing and production. All samples have a carbon footprint up to 23–55% lower than Portland cement. They are also more readily made and recycled. These materials are therefore more environmentally sustainable than Portland cement and could help to reduce CO_{2eq} emissions from the cement industry, and reduce heat demand in housing. The life cycle analysis presented here is simplistic, and more detailed life cycle and cost analyses should be the subject of future research to fully understand the economic impact of these materials in replacing Portland cement. However, the methodology adopted provides the basis for implementing a decision-making tool that can advise on, or scope in, low-carbon options before a more resource intensive life cycle assessment approach is applied. It will be therefore useful to construction companies or private developers intending to develop non-conventional building materials (e.g. geopolymers, alkali-activated cements), not yet regulated by law or international standards.

Acknowledgement

This work is supported by UK Engineering and Physical Sciences Research Council, (EPSRC Grant No. EP/L014041/1 - DISTINCTIVE Consortium - Decommissioning, Immobilisation and Storage soluTIons for NuClear wasTe InVEntories). Data associated with research published in this article is accessible at: https://doi.org/10.15129/b74bc130-e22d-4043-983b-9823139666f2.

Appendix A. Supplementary data

Supplementary data related to this article can be found at https://doi.org/10.1016/j.jclepro.2018.02.138.

References

Aggarwal, P., Singh, R.P., Aggarwal, Y., 2015. Use of nano-silica in cement based materialsA review. Cogent Eng. 2 (1), 1078018 https://doi.org/10.1080/23311916.2015.1078018.

Ahmed, A., Fried, A., 2012. Flexural strength of low density blockwork. Construct. Build. Mater. 35, 516–520. https://doi.org/10.1016/j.conbuildmat.2012.04.082.

Al-homoud, M.S., 2005. Performance characteristics and practical applications of common building thermal insulation materials. Build. Environ. 40, 353–366. https://doi.org/10.1016/j.buildenv.2004.05.013.

Al-Jabri, K.S., Hago, A.W., Al-Nuaimi, A.S., Al-Saidy, A.H., 2005. Concrete blocks for thermal insulation in hot climate. Cement Concr. Res. 35 (8), 1472–1479. https://doi.org/10.1016/j.cemconres.2004.08.018.

Alam, M., Singh, H., Brunner, S., Naziris, C., 2014. Experimental characterisation and evaluation of the thermo-physical properties of expanded perlite - fumed silica composite for effective vacuum insulation panel (VIP) core. Energy Build. 69, 442–450. https://doi.org/10.1016/j.enbuild.2013.11.027.

Aldawi, F., Alam, F., 2016. Residential Building Wall Systems. Elsevier Inc. https://doi.org/10.1016/B978-0-12-802397-6.00008-7

Alonso, S., Palomo, A., 2001. Alkaline activation of metakaolin and calcium hydroxide mixtures: influence of temperature, activator concentration and solids ratio. Mater. Lett. 47 (1–2), 55–62. https://doi.org/10.1016/S0167-577X(0000212-3).

Alvarez, F.X., Jou, D., Sellitto, A., 2010. Pore-size dependence of the thermal conductivity of porous silicon: a phonon hydrodynamic approach. Appl. Phys. Lett. 97 (3), 1–4. https://doi.org/10.1063/1.3462936.

Benhelal, E., Zahedi, G., Shamsaei, E., Bahadori, A., 2013. Global strategies and potentials to curb {CO}2 emissions in cement industry. J. Clean. Prod. 51 (0), 142–161. https://doi.org/10.1016/j.jclepro.2012.10.049.

Bull, J., Gupta, A., Mumovic, D., Kimpian, J., 2014. Life cycle cost and carbon footprint of energy efficient refurbishments to 20th century UK school buildings. Int. J. Sustain. Built Environ. 3 (1), 1–17. https://doi.org/10.1016/j.ijsbe.2014.07.002.

Chan, C.S., Thorpe, D., Islam, M., 2016. An evaluation carbon footprint in fly ash based geopolymer cement and ordinary Portland cement manufacture. In: IEEE International Conference on Industrial Engineering and Engineering Management 2016-Janua (1), pp. 254–259. https://doi.org/10.1109/IEEM.2015.7385647.

Cho, K., Hong, Y., Seo, J., 2014. Assessment of the economic performance of vacuum insulation panels for housing projects. Energy Build. 70, 45–51. https://doi.org/10.1016/j.enbuild.2013.11.073.

Cruz-Yusta, M., Mármol, I., Morales, J., Sánchez, L., 2011. Use of olive biomass fly ash in the preparation of environmentally friendly mortars. Environ. Sci. Technol. 45 (16), 6991–6996. https://doi.org/10.1021/es200968a.

Duxson, P., Provis, J.L., Lukey, G.C., van Deventer, J.S.J., 2007. The role of inorganic polymer technology in the development of 'green concrete'. Cement Concr. Res. 37 (12), 1590–1597. https://doi.org/10.1016/j.cemconres.2007.08.018.

EU, 2007. Reference Document on Best Available Techniques for the Manufacture of Large Volume Inorganic Chemicals - Silica and Others. European Commission BREF - LVI (August), pp. 1–711.

Fricke, J., Heinemann, U., Ebert, H.P., 2008. Vacuum insulation panels-From research to market. Vacuum 82 (7), 680–690. https://doi.org/10.1016/j.vacuum.2007.10.014.

Gameiro, A., Santos Silva, A., Faria, P., Grilo, J., Branco, T., Veiga, R., Velosa, A., 2014. Physical and chemical assessment of limemetakaolin mortars: influence of binder:aggregate ratio. Cement Concr. Compos. 45, 264–271. https://doi.org/10.1016/j.cemconcomp.2013.06.010.

Gao, K., Lin, K.-L., Wang, D., Hwang, C.-L., Anh Tuan, B.L., Shiu, H.-S., Cheng, T.-W., 2013. Effect of nano-SiO2 on the alkali-activated characteristics of metakaolin-based geopolymers. Construct. Build. Mater. 48, 441–447. https://doi.org/10.1016/j.conbuildmat.2013.07.027.

Garbev, K., Bornefeld, M., Beuchle, G., Stemmermann, P., 2008. Cell dimensions and composition of nanocrystalline calcium silicate hydrate solid solutions. Part 2: X-Ray and thermogravimetry study. J. Am. Ceram. Soc. 91 (9), 3015–3023. https://doi.org/10.1111/j.1551-2916.2008.02601.x.

Gomez-zamorano, L., Balonis, M., Erdemli, B., Neithalat, N., 2016. Structure, composition and thermochemical properties of C-(N)-S-H and N-A-S-H gels. In: 1st International Conference on Grand Challenges in Construction Materials, pp. 1–9.

Gomez-Zamorano, L., Balonis, M., Erdemli, B., Neithalath, N., Sant, G., 2017. C-(N)-S-H and N-A-S-H gels: compositions and solubility data at 25C and 50C. J. Am. Ceram. Soc. (May 2016), 2700–2711. https://doi.org/10.1111/jace.14715.

Grilo, J., Santos Silva, A., Faria, P., Gameiro, A., Veiga, R., Velosa, A., 2014. Mechanical and mineralogical properties of natural hydraulic lime-metakaolin mortars in different curing conditions. Construct. Build. Mater. 51, 287–294. https://doi.org/10.1016/j.conbuildmat.2013.10.045.

Hamilton, A., Hall, C., 2005. Physicochemical characterization of a hydrated calcium silicate board material. J. Build. Phys. 29 (1), 9–19. https://doi.org/10.1177/1744259105053280.

Hasanbeigi, A., Price, L., Lu, H., Lan, W., 2010. Analysis of energy-efficiency opportunities for the cement industry in Shandong Province, China: a case study of 16 cement plants. Energy 35 (8), 3461–3473. https://doi.org/10.1016/j.energy.2010.04.046.

Heidrich, C., Sanjayan, J., Berndt, M.L., Foster, S., 2015. Pathways and barriers for acceptance and usage of geopolymer concrete in mainstream construction. In: 2015 World of Coal Ash (WOCA) Conference in Nashville. Nashville.

Hemalatha, T., Mapa, M., George, N., Sasmal, S., 2016. Physico-chemical and mechanical characterization of high volume fly ash incorporated and engineered cement system towards developing greener cement. J. Clean. Prod. 125, 268–281. https://doi.org/10.1016/j.jclepro.2016.03.118.

Hienola, A., Pietikäinen, J.-P., Donnell, D.O., Partanen, A.-I., Korhonen, H., 2017. The role of anthropogenic aerosol emission reduction in achieving the Paris Agreement 's objective. Geophys. Res. Abstr. 19. EGU2017-12544.

Imbabi, M.S., Carrigan, C., McKenna, S., 2012. Trends and developments in green cement and concrete technology. Int. J Sustain. Built Environ. 1 (2), 194–216. https://doi.org/10.1016/j.ijsbe.2013.05.001.

IPCC, 2006. Chapter 2: Mineral Industry Emissions, 2006 IPCC Guidelines for National Greenhouse Gas Inventories, vol. 3, p. 40.

Kajaste, R., Hurme, M., 2016. Cement industry greenhouse gas emissions - management options and abatement cost. J. Clean. Prod. 112, 4041–4052. https://doi.org/10.1016/j.jclepro.2015.07.055.

Lazaro, A., Quercia, G., Brouwers, H.J.H., Geus, J.W., 2013. Synthesis of a Green nano-silica material using beneficiated waste dunites and its application in concrete. World J. Nano Sci. Eng. 03 (03), 41–51. https://doi.org/10.4236/wjnse.2013.33006.

Lazaro, A., Yu, Q., Brouwers, H., 2016. 4 Nanotechnologies for sustainable construction. Sustain. Constr. Mater. 55–78. https://doi.org/10.1016/B978-0-08-100370-1.00004-4.

Lin, Q., Lan, X., Li, Y., Ni, Y., Lu, C., Chen, Y., Xu, Z., 2010. Preparation and characterization of novel alkali-activated nano silica cements for biomedical application. J. Biomed. Mater. Res. Part B Appl. Biomater. 95 (2), 347–356. https://doi.org/10.1002/jbm.b.31722.

Loudon, A.G., 1979. The thermal properties of lightweight concretes. Int. J. Cement Composit. Lightweight Concrete 1 (2), 71–85. https://doi.org/10.1016/0262-5075(7990013-7).

McLellan, B.C., Williams, R.P., Lay, J., van Riessen, A., Corder, G.D., 2011. Costs and carbon emissions for geopolymer pastes in comparison to ordinary portland cement. J. Clean. Prod. 19 (9–10), 1080–1090. https://doi.org/10.1016/j.jclepro.2011.02.010.

Mellado, A., Catalán, C., Bouzón, N., Borrachero, M.V., Monzó, J.M., Payá, J., 2014. Carbon footprint of geopolymeric mortar: study of the contribution of the alkaline activating solution and assessment of an alternative route. RSC Adv. 4, 23846–23852. https://doi.org/10.1039/c4ra03375b.

Moretti, L., Caro, S., 2017. Critical analysis of the life cycle assessment of the Italian cement industry. J. Clean. Prod. 152, 198–210. https://doi.org/10.1016/j.jclepro.2017.03.136.

Nath, S., Maitra, S., Mukherjee, S., Kumar, S., 2016. Microstructural and morphological evolution of fly ash based geopolymers. Construct. Build. Mater. 111, 758–765. https://doi.org/10.1016/j.conbuildmat.2016.02.106.

Nie, Q., Hu, W., Ai, T., Huang, B., Shu, X., He, Q., 2016. Strength properties of geopolymers derived from original and desulfurized red mud cured at ambient temperature. Construct. Build. Mater. 125, 905–911. https://doi.org/10.1016/j.conbuildmat.2016.08.144.

Palmero, P., Formia, A., Antonaci, P., Brini, S., Tulliani, J.M., 2015. Geopolymer technology for application-oriented dense and lightened materials. Elaboration and characterization. Ceram. Int. 41 (10), 12967–12979. https://doi.org/10.1016/j.ceramint.2015.06.140.

Papadopoulos, A.M., Giama, E., 2007. Environmental performance evaluation of thermal insulation materials and its impact on the building. Build. Environ. 42 (5), 2178–2187. https://doi.org/10.1016/j.buildenv.2006.04.012.

Prakash, T.M., Naresh, B.G., Karisiddappa, B.G., Raghunath, S., 2013. Properties of aerated (foamed) concrete blocks. Int. J. Sci. Eng. Res. 4 (1), 1–5.

Proietti, S., Desideri, U., Sdringola, P., Zepparelli, F., 2013. Carbon footprint of a reflective foil and comparison with other solutions for thermal insulation in building envelope. Appl. Energy 112, 843–855. https://doi.org/10.1016/j.apenergy.2013.01.086.

Reffold, E., Leighton, F., Choudhury, F., Rayner, P.S., 2008. Greenhouse Gas Emissions of Water Supply and Demand Management Options. Tech. rep.. Environment Agency.

Reig, L., Soriano, L., Borrachero, M., Monzó, J., Payá, J., 2016. Influence of calcium aluminate cement (CAC) on alkaline activation of red clay brick waste (RCBW). Cement Concr. Compos. 65, 177–185. https://doi.org/10.1016/j.cemconcomp.2015.10.021.

Rostami, H., Brendley, W., 2003. Alkali ash material: a novel fly ash-based cement. Environ. Sci. Technol. 37 (15), 3454–3457. https://doi.org/10.1021/es026317b.

Salas, D.A., Ramirez, A.D., Rodríguez, C.R., Petroche, D.M., Boero, A.J., Duque-Rivera, J., 2016. Environmental impacts, life cycle assessment and potential improvement measures for cement production: a literature review. J. Clean. Prod. 113, 114–122. https://doi.org/10.1016/j.jclepro.2015.11.078.

Sanchez, F., Ince, C., 2009. Microstructure and macroscopic properties of hybrid carbon nanofiber/silica fume cement composites. Compos. Sci. Technol. 69 (7–8), 1310–1318. https://doi.org/10.1016/j.compscitech.2009.03.006.

Schneider, M., Romer, M., Tschudin, M., Bolio, H., 2011. Sustainable cement production present and future. Cement Concr. Res. 41 (7), 642–650. https://doi.org/10.1016/j.cemconres.2011.03.019.

Silva, A.S., Gameiro, A., Grilo, J., Veiga, R., Velosa, A., 2014. Long-term behavior of limemetakaolin pastes at ambient temperature and humid curing condition. Appl. Clay Sci. 88, 49–55. https://doi.org/10.1016/j.clay.2013.12.016.

Stafford, F.N., Dias, A.C., Arroja, L., Labrincha, J.A., Hotza, D., 2016. Life cycle assessment of the production of Portland cement: a Southern Europe case study. J. Clean. Prod. 126, 159–165. https://doi.org/10.1016/j.jclepro.2016.02.110.

Stafford, F.N., Raupp-Pereira, F., Labrincha, J.A., Hotza, D., 2016. Life cycle assessment of the production of cement: a Brazilian case study. J. Clean. Prod. 137, 1293–1299. https://doi.org/10.1016/j.jclepro.2016.07.050.

Sturm, P., Gluth, G.J.G., Brouwers, H.J.H., Kühne, H.C., 2016. Synthesizing one-part geopolymers from rice husk ash. Construct. Build. Mater. 124, 961–966. https://doi.org/10.1016/j.conbuildmat.2016.08.017.

Taylor, H., 1998. Cement Chemistry, second ed., vol. 20. https://doi.org/10.1016/S0958-9465(9800023-7)

Turner, L.K., Collins, F.G., 2013. Carbon dioxide equivalent (CO2-e) emissions: a comparison between geopolymer and OPC cement concrete. Construct. Build. Mater. 43, 125–130. https://doi.org/10.1016/j.conbuildmat.2013.01.023.

Ünal, O., Uygunolu, T., Yildiz, A., 2007. Investigation of properties of low-strength lightweight concrete for thermal insulation. Build. Environ. 42 (2), 584–590. https://doi.org/10.1016/j.buildenv.2005.09.024.

Industrial Decarbonisation & Energy Efficiency Roadmaps to 2050 - Cement, 2015. Department for Business, Innovation & Skills and Department of Energy & Climate Change.

Villaquiran-Caicedo, M.A., de Gutierrez, R.M., Sulekar, S., Davis, C., Nino, J.C., 2015. Thermal properties of novel binary geopolymers based on metakaolin and alternative silica sources. Appl. Clay Sci. 118, 276–282. https://doi.org/10.1016/j.clay.2015.10.005.

World Business Council for Sustainable Development (WBCSD), 2011. CO2 and Energy Accounting and Reporting Standard for the Cement Industry. Tech. Rep. May.

World Business Council for Sustainable Development (WBCSD), International Energy Agency (IEA), Cement Roadmap, 2009.

Wu, Y., Wang, J.Y., Monteiro, P.J.M., Zhang, M.H., 2015. Development of ultra-lightweight cement composites with low thermal conductivity and high specific strength for energy efficient buildings. Construct. Build. Mater. 87,

100–112. https://doi.org/10.1016/j.conbuildmat.2015.04.004.
Yu, K.N., Balendran, R.V., Koo, S.Y., Cheung, T., 2000. Silica fume as a radon retardant from concrete. Environ. Sci. Technol. 34 (11), 2284–2287. https://doi.org/10.1021/es991134j.
Zhang, Z., Wang, H., Provis, J.L., Bullen, F., Reid, A., Zhu, Y., 2012. Quantitative kinetic and structural analysis of geopolymers. Part 1. the activation of metakaolin with sodium hydroxide. Thermochim. Acta 539, 23–33. https://doi.org/10.1016/j.tca.2012.03.021.
Zhang, Z., Provis, J.L., Reid, A., Wang, H., 2014. Geopolymer foam concrete: an emerging material for sustainable construction. Construct. Build. Mater. 56, 113–127. https://doi.org/10.1016/j.conbuildmat.2014.01.081.
Zhang, J., He, Y., Wang, Y.-P., Mao, J., Cui, X.-M., 2014. Synthesis of a self-supporting faujasite zeolite membrane using geopolymer gel for separation of alcohol/water mixture. Mater. Lett. 116, 167–170. https://doi.org/10.1016/j.matlet.2013.11.008.